Three-Dimensional Solution Structure of the N-Terminal Receiver Domain of NTRC†,‡

Brian F. Volkman,§,|| Michael J. Nohaile,||,⊥ Nancy K. Amy,# Sydney Kustu,⊥ and David E. Wemmer*,§,||

Department of Molecular and Cell Biology, Department of Chemistry, and Department of Nutritional Sciences, University of California, and the Structural Biology Division, Lawrence Berkeley Laboratory, 1 Cyclotron Road, Berkeley, California 94720

Received September 19, 1994; Revised Manuscript Received November 15, 1994⊗

ABSTRACT: NTRC is a transcriptional enhancer binding protein whose N-terminal domain is a member of the family of receiver domains of two-component regulatory systems. Using 3D and 4D NMR spectroscopy, we have completed the ^{1}H, ^{15}N, and ^{13}C assignments and determined the solution structure of the N-terminal receiver domain of the NTRC protein. Determination of the three-dimensional structure was carried out with the program X-PLOR (Brünger, 1992) using a total of 915 NMR-derived distance and dihedral angle restraints. The resultant family of structures has an average root mean square deviation of 0.81 Å from the average structure for the backbone atoms involved in well-defined secondary structure. The structure is comprised of five α-helices and a five-stranded parallel β-sheet, in a $(\beta/\alpha)_5$ topology. Comparison of the solution structure of the NTRC receiver domain with the crystal structures of the homologous protein CheY in both the Mg^{2+}-free and Mg^{2+}-bound forms [Stock, A. M., Mottonen, J. M., Stock, J. B., & Schutt, C. E. (1989) *Nature 337*, 745−749; Volz, K., & Matsumura, P. (1991) *J. Biol. Chem. 296*, 15511−15519; Stock, A. M., Martinez-Hackert, E., Rasmussen, B. F., West, A. H., Stock, J. B., Ringe, D., & Petsko, G. A. (1993) *Biochemistry 32*, 13375−13380; Bellsolell, L., Prieto, J., Serrano, L., & Coll, M. (1994) *J. Mol. Biol. 238*, 489−495] reveals a very similar fold, with the only significant difference occurring in the positioning of helix 4 relative to the rest of the protein. Examination of the conformation of consensus residues of the receiver domain superfamily [Volz, K. (1993) *Biochemistry 32*, 11741−11753] in the structures of the NTRC receiver domain and CheY establishes the structural importance of residues whose side chains are involved in hydrogen bonding or hydrophobic core interactions. The importance of some nonconsensus residues which may be conserved for their ability to fulfill helix capping roles is also discussed.

"Two-component" signal transduction pathways are remarkably common in eubacterial responses to changes in local environment (Parkinson & Kofoid, 1992) and have recently been identified in eukaryotic cells (Chang et al., 1993; Ota & Varshavsky, 1993; Maeda et al., 1994). Such two-component pathways are involved in a wide array of processes, such as nitrogen regulation, chemotaxis, and osmoregulation. The archetypal system consists of a histidine kinase and a response regulator or receiver domain. The histidine kinase autophosphorylates, often in response to an environmental stimulus. The phosphate incorporated is then transferred from the histidine in the autokinase to an aspartate residue in the receiver domain of the cognate second component. The phosphorylated receiver domain modulates the function of an attached output domain or, rarely, a separate protein.

In the case of nitrogen regulation, the phosphorylation of D54 in the amino (N)-terminal domain of the NTRC[1] protein, the receiver domain in this system, is accomplished via a phosphotransfer reaction from the histidine kinase, NTRB (Ninfa & Magasanik, 1986; Keener & Kustu, 1988; Weiss & Magasanik, 1988; Sanders et al., 1992). The phosphorylation of D54 in the N-terminal domain of NTRC is required for activation of an ATPase in the central domain of the protein (Weiss et al., 1991; Austin & Dixon, 1992). This, in turn, allows NTRC to catalyze the formation of open complexes between the σ^{54}-holoenzyme form of RNA polymerase and promoters, resulting in the transcription of genes whose products participate in nitrogen metabolism. Phosphorylation of the N-terminal domain of NTRC is not required for its DNA-binding per se but induces oligomerization of NTRC dimers at enhancers, which are composed of two NTRC binding sites. Activation of the ATPase is thought to be mediated by this oligomerization (Austin &

† We are grateful to the Office of Energy Research, Office of Health and Environmental Research, Health Effects Research Division of the U.S. Department of Energy under Contract No. DE-AC03-76SF00098 for research support. Instrumentation grants from the U.S. Department of Energy, DE FG05-86ER75281, and the National Science Foundation, DMB 86-09035 and BBS 87-20134, are also gratefully acknowledged.

‡ The coordinates for the 20 final structures of the NTRC receiver domain have been deposited in the Brookhaven Protein Data Bank with the identification code 1NTR.

* To whom correspondence should be addressed.

§ Department of Chemistry, University of California, Berkeley.

|| Structural Biology Division, Lawrence Berkeley Laboratory.

⊥ Department of Molecular and Cell Biology, University of California, Berkeley.

Department of Nutritional Sciences, University of California, Berkeley.

⊗ Abstract published in *Advance ACS Abstracts,* January 1, 1995.

[1] Abbreviations: NTRC, nitrogen regulatory protein C; NMR, nuclear magnetic resonance; TSP, sodium 3-(trimethylsilyl)propionate; NOE, nuclear Overhauser effect; NOESY, NOE spectroscopy; TOCSY, total correlation spectroscopy; HMQC, heteronuclear multiple-quantum coherence; HSQC, heteronuclear single-quantum coherence; TPPI, time-proportional phase incrementation; RMSD, root mean square deviation; DGSA, distance geometry/simulated annealing; 4D NOESY, four-dimensional ^{13}C-edited HMQC-NOESY-HMQC.

0006-2960/95/0434-1413$09.00/0

Dixon, 1992; Weiss, V., et al., 1992; Porter, 1993; Porter et al., 1995). Unlike phosphorylation, deletion of the receiver domain of NTRC fails to activate the ATPase of the central domain (Drummond et al., 1990; Weiss, D., et al., 1992).

The three-dimensional structure of CheY, a member of the receiver domain superfamily, has been solved by X-ray crystallography and NMR spectroscopy, with and without Mg^{2+} bound (Stock et al., 1989, 19933; Volz & Matsumura, 1991; Bellsolell et al., 1994; Moy et al., 1994). Mutational analysis and sequence comparisons have indicated that the side chains of residues D12, D13, D57, T87, and K107 form the active site of CheY, with D57 the site of phosphorylation (Lukat et al., 1991; Volz, 1993). Receiver domains themselves catalyze phosphate incorporation from their cognate autokinases and from low molecular weight donors such as carbamyl phosphate, acetyl phosphate, and phosphoramidate (Feng et al., 1992; Lukat et al., 1992). In addition, a number of them have been shown to have an autophosphatase activity (Hess et al., 1988; Keener & Kustu, 1988). CheY, in contrast to most two-component receiver domains, is a single domain protein that interacts with its target(s) in the switch complex of the flagellar motor to control the direction of flagellar rotation (Ravid et al., 1986). By contrast, NTRC, like most other members of the superfamily, contains the N-terminal receiver domain and its downstream target within the same protein. Differences in the structures of CheY and the N-terminal domain of NTRC may indicate regions important for the interaction of these receiver domains with their respective downstream targets.

The important regulatory role of receiver domains of two-component systems raises many questions about relationships between structure and function. Of primary interest are the structural rearrangements postulated to occur upon phosphorylation and communication to downstream targets via these rearrangements. Determination of the three-dimensional structure of the receiver domain of NTRC is a step toward obtaining detailed information on the mechanism of signal transduction from this domain to the central domain of the protein. In this article we report the NMR assignments and three-dimensional solution structure of the N-terminal receiver domain of the NTRC protein from *Salmonella typhimurium* and discuss differences from CheY.

MATERIALS AND METHODS

Expression, Purification, and Enzymatic Activity of the NTRC Receiver Domain. The expression vector pJES592 (Klose et al., 1994), which includes a T7 promoter and a DNA fragment encoding the N-terminal domain of NTRC (residues 1−124), was transformed into *Escherichia coli* BL21(DE3) cells carrying the pLysS plasmid (Studier et al., 1990). In order to obtain uniform labeling of protein samples, cells were grown on M9 minimal medium (Sambrook et al., 1989) at 37 °C with $^{15}NH_4Cl$ and [$^{13}C_6$]D-glucose as the sole sources of nitrogen and carbon, respectively. NTRC receiver domain selectively labeled with [^{15}N]leucine was grown similarly, but with the addition of the other 19 naturally occurring amino acids at a concentration of 100 mg/L and the isotopically enriched amino acid at 150 mg/L. Production of the NTRC receiver domain was induced with the addition of 1 mM isopropyl β-D-thiogalactopyranoside after the cell density had reached 0.25 absorbance units at 595 nm. The cells were grown for 9−12 h after induction, whereupon they were harvested by centrifugation. The cells were lysed by sonication in lysis bufer (100 mM KCl, 50 mM Tris-acetate, pH 8.2, 5% glycerol), and a crude extract was prepared by centrifugation at 20 000 rpm for 20 min in an SW28 rotor. The supernatant was diluted 2-fold and applied to a DEAE Sephadex-50 column. The column was washed with five column volumes of running buffer (50 mM NaCl, 10 mM phosphate, pH 6.8, 0.5 mM dithiothreitol) and eluted in a stepped gradient of increasing salt concentration (50−500 mM NaCl in 50 mM increments of 30 mL). The NTRC receiver domain elutes at 250−300 mM NaCl. The fractions containing NTRC receiver domain were concentrated using Centriprep-10 (Amicon) flow concentrators. Final HPLC purification was performed on a 5PW DEAE ion exchange column (Waters). Purity and identity of the protein were confirmed by mass spectroscopy and NMR.

The rate of phosphorylation of the receiver domain and its steady-state level of phosphorylation, which represents a balance between phosphate incorporation and release, were checked with 1 μM NTRC receiver domain [preparations before and after lyophilization (see below)] and 200 nM NTRB as described (Keener & Kustu, 1988). Activities of the receiver domain were similar to those of intact NTRC and a maltose-binding protein fusion to the receiver domain, verifying that preparations used for NMR spectroscopy had normal enzymatic activity.

Sample Preparation. Concentrated protein solution was flow dialyzed against 10 mM phosphate buffer, pH 6.4, and lyophilized. Dry protein samples were dissolved in 0.5 mL of D_2O or 10% D_2O/90% H_2O. The pH of NMR samples was adjusted to 6.4 with 1 M HCl or NaOH. The concentrations of the uniformly ^{15}N-labeled and [^{15}N]Leu-labeled samples were 2 mM; the concentration of the uniformly ^{13}C,^{15}N-labeled sample was 3 mM. The concentrations of NMR samples are based on the weight of the lyophilized material after HPLC purification and dialysis against water.

NMR Experiments. NMR experiments were performed at 600 MHz on a Bruker AMX-600 spectrometer at 25 °C. Chemical shift values were externally referenced to TSP (^{1}H and ^{13}C) (Driscoll et al., 1990) and liquid ammonia (^{15}N) (Live et al., 1984). Nonacquisition dimensions of all multidimensional experiments utilized the States−TPPI method for quadrature detection (Marion et al., 1989a). All data were processed with FELIX version 2.30β (Biosym), including linear prediction calculations. Shifted skewed sine-bell functions were used for apodization of the free induction decays.

^{15}N-edited 3D NOESY-HMQC (Kay et al., 1989; Marion et al., 1989b), and 3D TOCSY-HMQC (Driscoll et al., 1990) experiments were collected with spectral widths of 6944 Hz for the ^{1}H dimensions and 1861 Hz for the ^{15}N dimension. The ^{1}H carrier was placed on the H_2O resonance at 4.80 ppm and the ^{15}N carrier set to 116.2 ppm. The NOESY mixing time was 100 ms, and the TOCSY spin-lock period was 80 ms. A total of 128 × 32 × 1024 complex points were collected in the t_1, t_2, and t_3 dimensions, respectively. Data were apodized in each dimension with a shifted, skewed sine-bell. A shift of 75° was used in each dimension, with a skew of 1.0, 0.8, and 0.5 in the t_1, t_2, and t_3 dimensions, respectively. Data were zero-filled to yield a 512 × 64 × 512 real matrix upon Fourier transformation.

^{15}N−^{1}H 2D HSQC (Bodenhausen & Ruben, 1980; Marion et al., 1989a) experiments were collected with identical

spectral parameters, but 256 complex points were acquired in the ^{15}N dimension to yield a high-resolution spectrum for assignment purposes. A 2D HMQC-J experiment was collected with similar parameters to the HSQC experiments, but with 498 complex points in order to obtain $J^3_{H\alpha-HN}$ values used to generate qualitative dihedral angle restraints (Kay & Bax, 1990). The $^{15}N-^1H$ HSQC experiment also provided amide exchange information from a sample dissolved in D_2O immediately prior to acquisition of a series of 2D experiments.

2D $^1H-^{13}C$ HSQC experiments were collected for both the aliphatic and aromatic resonances of the NTRC receiver domain, using a constant-time (CT) evolution period for ^{13}C equal to $1/J_{CC}$, producing a completely ^{13}C-decoupled spectrum in t_1 (Vuister & Bax, 1992). The aromatic CT-HSQC was centered at 122.64 ppm ^{13}C, with a ^{13}C spectral width of 3968 Hz, and at 4.80 ppm ^1H, with a ^1H spectral width of 7246 Hz. The aliphatic CT-HSQC was centered at 43.16 ppm ^{13}C with a ^{13}C spectral width of 5000 Hz and at 4.80 ppm ^1H with a ^1H spectral width of 7246 Hz. After normal processing, $^1H-^{13}C$ HSQC spectra were treated with an average noise measurement routine, ANI, and a t_1 noise reduction routine, RT1, to attenuate the streaking of intense methyl and aromatic signals, which tended to obscure weaker peaks (Manoleras & Norton, 1992). Postprocessing with ANI and TR1 used a threshold value, T, of 5 and a spread value, η, of 3.0 with 10 iterations.

A 3D ^{13}C HCCH-TOCSY experiment (Bax et al., 1990) was acquired with parameters identical to the ^1H dimension of the aliphatic 2D CT-HSQC, but in the ^{13}C dimension only 27 complex points were collected with a spectral width of 2809 Hz, centered at 43.16 ppm. Extensive ^{13}C aliasing was used to maintain reasonably high resolution, despite the low digitization in that dimension. Methyl resonances which appear above 18.39 ppm in the ^{13}C dimension were aliased to values two spectral widths downfield. A total of 128 complex points were collected in the t_1 ^1H dimension and zero-filled to yield a 256 × 64 × 512 real matrix.

A 4D ^{13}C HMQC-NOESY-HMQC experiment (Clore et al., 1991) with a 100 ms mixing time was used to generate distance restraints between carbon-bound protons. Eight complex points in each of the two ^{13}C dimensions (t_1 and t_3), 56 points in the t_2 dimension, and 256 points in the t_4 dimension were acquired over 76 h. Both ^1H dimensions were centered at 4.13 ppm with spectral widths of 5319 Hz. The ^{13}C dimensions were centered at 43.16 ppm with spectral widths of 2809 Hz. In processing the data, both ^1H dimensions were processed normally, followed by Fourier transformation of the t_3 ^{13}C dimension without apodization. The t_1 ^{13}C dimension was then linear predicted to 12 complex points, apodized, and Fourier transformed, followed by inverse transformation of the t_3 dimension, linear prediction, apodization, and Fourier transformation. The time domain data were zero-filled to produce a 16 × 128 × 16 × 256 real matrix.

A 3D CBCA(CO)NH (Grzesiek & Bax, 1992) experiment was collected with ^1H and ^{15}N parameters identical to the 3D ^{15}N experiments described above. The ^{13}C dimension was centered at 43.16 ppm with a spectral width of 8446 Hz. Fifty complex points were collected in the ^{13}C dimension and linear predicted to 75 points. Time-domain data were zero-filled to yield a 256 × 64 × 512 real matrix.

Structure Calculations. Structure calculations were performed using the program X-PLOR 3.1 (Brünger, 1992). A standard protocol for embedding, annealing, and optimizing the coordinates was used (Nilges et al., 1988; Brünger, 1992). The *dg_sub_embed* routine was used to generate starting structures with substructures embedded from the smoothed bounds matrix. Molecular dynamics and simulated annealing were performed with the *dgsa* routine, and the *refine* routine was used for final optimization of structures. Distance restraints were generated from the cross peaks of both the ^{15}N 3D NOESY-HMQC and the ^{13}C HCCH-NOESY, and classified as strong (1.8−2.7 Å), medium (1.8−3.5 Å), and weak (1.8−5 Å) (Williamson et al., 1985; Clore et al., 1986). Corrections were added to the upper bounds of restraints involving pseudoatoms for methylene and methyl groups as well as Tyr and Phe ring protons (Wüthrich et al., 1983; Clore et al., 1986).

Dihedral angle restraints for selected ϕ angles were included on the basis of $J^3_{H\alpha-HN}$ coupling constants measured as splittings in the t_1 dimension of the HMQC-J experiment. For large values of $J^3_{H\alpha-HN}$ (>8 Hz) ϕ angles were constrained to $-120° \pm 40°$, and for small values (<6 Hz) ϕ angles were constrained to $-60° \pm 30°$, if the residue was known to fall in a helical region of the protein, since other values of ϕ may give rise to small $J^3_{H\alpha-HN}$ values.

Structure refinement was performed in an iterative fashion, using the current level of refinement to screen potential distance constraints on the basis of proximity in the structure. Hydrogen bonds were included as pairs of constraints between NH and N atoms to the corresponding carbonyl O atom, but only when NOE patterns indicated unambiguous donor−acceptor pairs and if the NH was observed in $^{15}N-^1H$ HSQC spectra collected at least 1 h after dissolving the sample in D_2O. Hydrogen bonds were defined by restraints defining the O−N distance to be between 2.8 and 3.3 Å and the O−H distance to be between 1.8 and 2.3 Å.

RESULTS

Resonance Assignments. Figure 1 shows the $^{15}N-^1H$ HSQC spectrum of the NTRC receiver domain, with assigned peaks labeled by residue and number. The single set of resonances with narrow line widths is consistent with the NTRC receiver domain being monomeric in solution at the concentrations used. Sequence-specific assignment of ^1H and ^{15}N resonances was completed using primarily the ^{15}N 3D NOESY-HMQC and ^{15}N 3D TOCSY-HMQC data collected from uniformly ^{15}N-labeled protein. The separation of spin systems by their amide ^{15}N chemical shift allows the straightforward identification of sequential αH−NH, NH−NH, and βH−NH NOEs for assignment of residues in a traditional manner (Wüthrich, 1986). Figure 2 contains selected strips from the ^{15}N 3D NOESY-HMQC and ^{15}N 3D TOCSY-HMQC experiments, illustrating the method by which ^{15}N-directed sequential assignments were made. The wide αH chemical shift dispersion which simplified much of the sequential assignment is also visible in Figure 2, with cross peaks from W7 Hα (6.55 ppm) and V39 Hα (2.84 ppm) indicated. Additional assignments were aided by comparison of the HSQC spectrum of [^{15}N]Leu-labeled protein with the uniformly labeled spectrum to unambiguously determine the residue type for those unassigned leucine residues. A number of $^{15}N-^1H$ correlations are not observed,

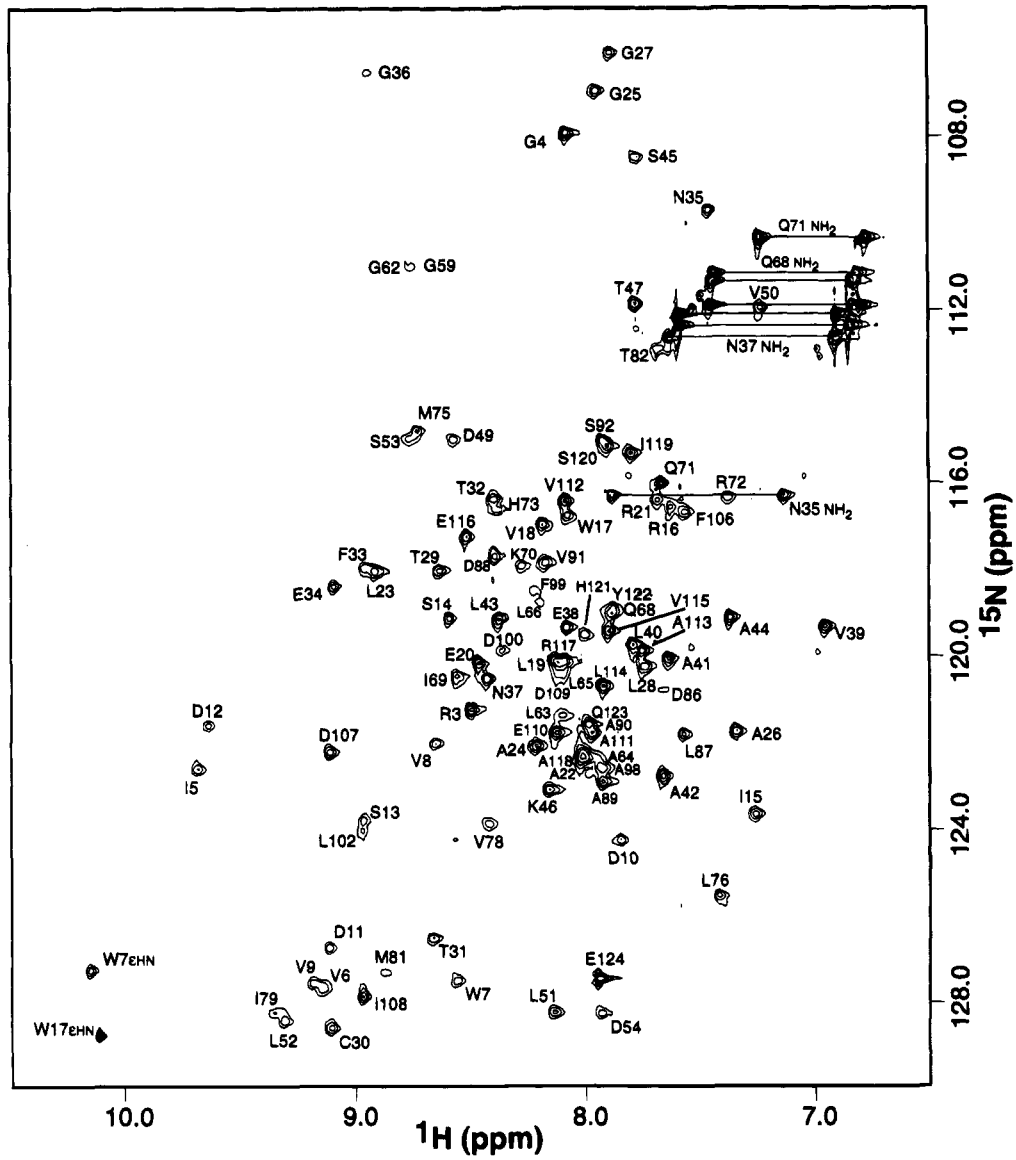

FIGURE 1: $^{1}H-^{15}N$ HSQC spectrum of uniformly ^{15}N-labeled NTRC receiver domain. Cross-peak assignments are indicated with the one-letter amino acid code and residue number.

possibly due to high exchange rates at near-neutral pH. A total of 85% of all backbone amide ^{15}N and ^{1}H resonances were assigned from these data, and a significant portion of the αH and side chain protons were assigned from the ^{15}N 3D TOCSY-HMQC spectrum.

One plane of the ^{13}C 3D HCCH-TOCSY experiment is shown in Figure 3. In order to assign the aliphatic ^{13}C resonances in the protein and complete the side chain ^{1}H assignments, $^{13}C-^{1}H\alpha$ peaks from the CT-HSQC experiment were correlated with spin systems in the ^{13}C 3D HCCH-TOCSY and then matched with Hα and side chain assignments from the ^{15}N 3D TOCSY-HMQC spectrum. Analysis of the 3D CBCA(CO)NH experiment correlated $^{13}C\alpha$ and $^{13}C\beta$ resonances with the ^{15}N and ^{1}H resonances of the following sequential residue, providing additional $^{13}C\alpha$ and $^{13}C\beta$ assignments for prolines and some residues whose $^{15}N-^{1}H$ correlations were not observed. These additional assignments were matched with unassigned spin systems remaining in the ^{13}C 3D HCCH-TOCSY data. Chemical shift values for most resonances were tabulated from peaks in the high-resolution HSQC experiments, with the remainder measured in the ^{13}C 3D HCCH-TOCSY or ^{13}C 4D NOESY data.

The 4D ^{13}C HMQC-NOESY-HMQC (4D NOESY) experiment was used to identify connections between proline residues and the preceding residues, as αH−αH or αH−δH sequential NOEs are observed for five of the six proline residues of the NTRC receiver domain. The conserved *cis*-peptide bond between K104 and P105 was confirmed in this manner, in agreement with the crystal structures of CheY. The exception is P48, for which complete resonance assignments were not obtained. Its $^{13}C\alpha$ and $^{13}C\beta$ chemical shifts were determined by correlation with the NH of D49 in the CBCA(CO)NH experiment, but it appears to be highly degenerate with other spin systems in the ^{13}C 3D HCCH-TOCSY. No NOEs to P48 could be identified which would confirm either the *cis* or *trans* form of the T47−P48 peptide bond; however, the value of the $^{13}C\beta$ chemical shift has been shown to be a reliable indicator of proline peptide bond isomerization (Scanlon & Norton, 1994). The value observed for the $^{13}C\beta$ of P48 is 30.35 ppm, in agreement with the value of 30.6 ppm reported for proline in a *trans* configuration (Dorman & Bovey, 1973; Wüthrich, 1976).

The 4D NOESY was also helpful in confirming assignments of aromatic ^{13}C and ^{1}H resonances, by identifying

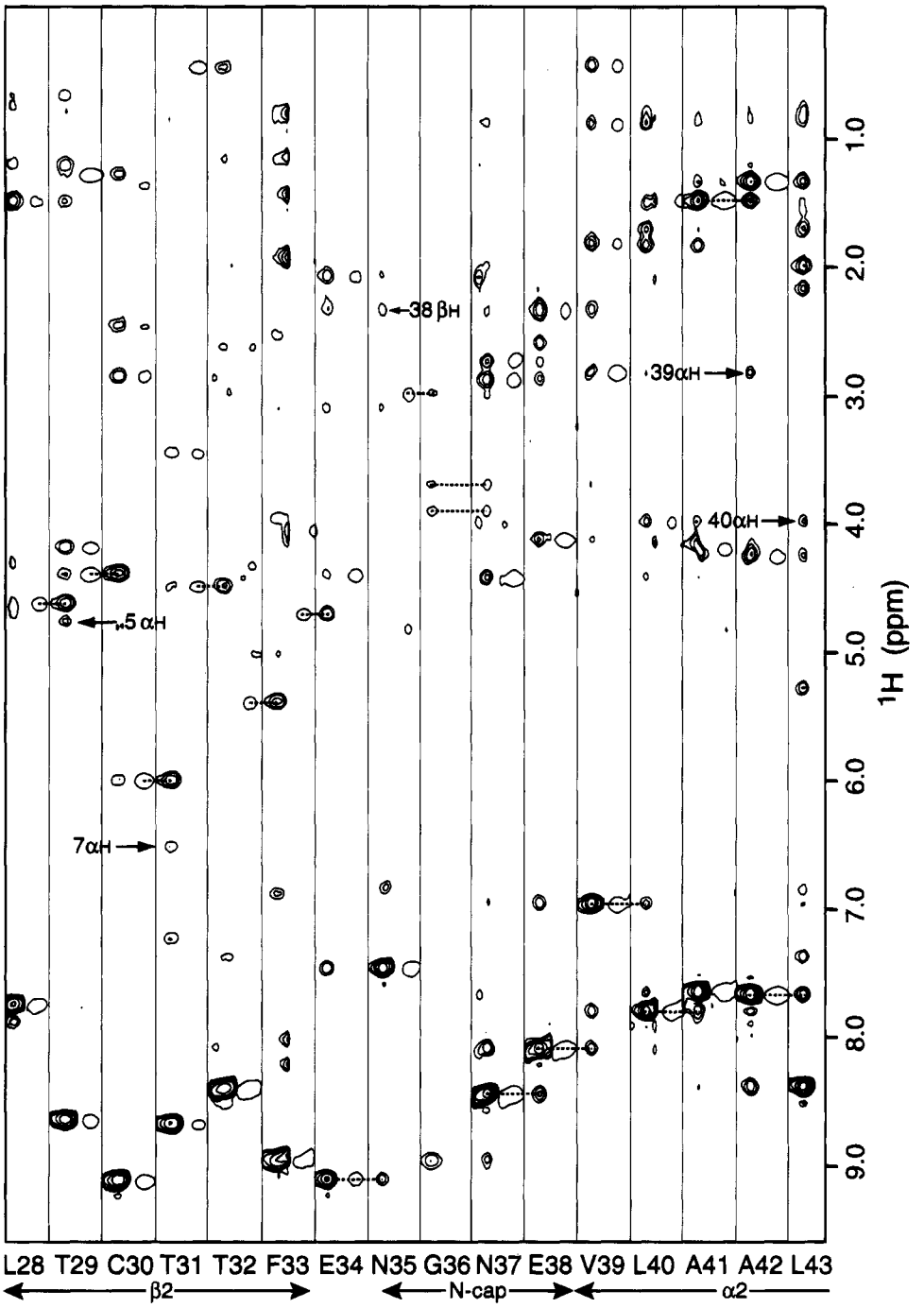

FIGURE 2: Strip plot of selected regions of the 3D ^{15}N NOESY-HMQC and TOCSY-HMQC spectra of NTRC receiver domain illustrating the sequential resonance assignments for residues 28−43. Each pair of vertical strips is taken from the 3D ^{1}H−^{1}H plane whose ^{15}N value is the amide nitrogen chemical shift of the amino acid listed on the horizontal axis. Strips are centered in F_3 at the amide proton chemical shift of the assigned residue. NOESY and TOCSY strips are alternated, with NOESY peaks displayed with multiple contours and TOCSY peaks drawn with a single contour. Sequential connectivities are indicated with dashed lines between TOCSY and NOESY peaks of neighboring residues. Residues 28−34 and 35−36 are connected by αH−NH NOEs; residues 34−35, 37−41, and 42−43 are connected by NH−NH NOEs; residues 41−42 are connected by a βH−NH NOE, due to the degeneracy of their amide protons. Labeled arrows denote cross peaks due to medium- and long-range NOEs between the specified proton and the amide proton of the residue indicated on the horizontal axis. Cross peaks from residues 5−29 and 7−31 are due to cross-strand NOEs in the parallel β-sheet structure. A βH−NH NOE from E38 to N35 is indicative of an N-capping interaction in helix 2. Helical αH−NH(i,i+3) NOEs from 39 to 42 and 40 to 43 are also shown.

strong cross peaks between aromatic protons and assigned βH resonances of aromatic residues. Tentative assignments from the 4D NOESY were compared with peaks in the aromatic ^{13}C CT-HSQC spectrum to confirm that ^{13}C values were in the appropriate ranges for the various types of aromatic side chains. The ^{1}H, ^{15}N, and ^{13}C chemical shift assignments for the receiver domain of NTRC at pH 6.4 and 25 °C can be obtained as supplementary material. In total, more than 90% of all ^{1}H, ^{15}N, and ^{13}C resonances of NTRC receiver domain were assigned sequence-specifically, with unobserved backbone amides and the corresponding side chains being the majority of missing assignments.

Identification of Secondary Structure. The location of secondary structure elements was determined initially by analysis of NOE patterns in the ^{15}N 3D NOESY-HMQC data. Figure 4 presents a summary of sequential and medium-range

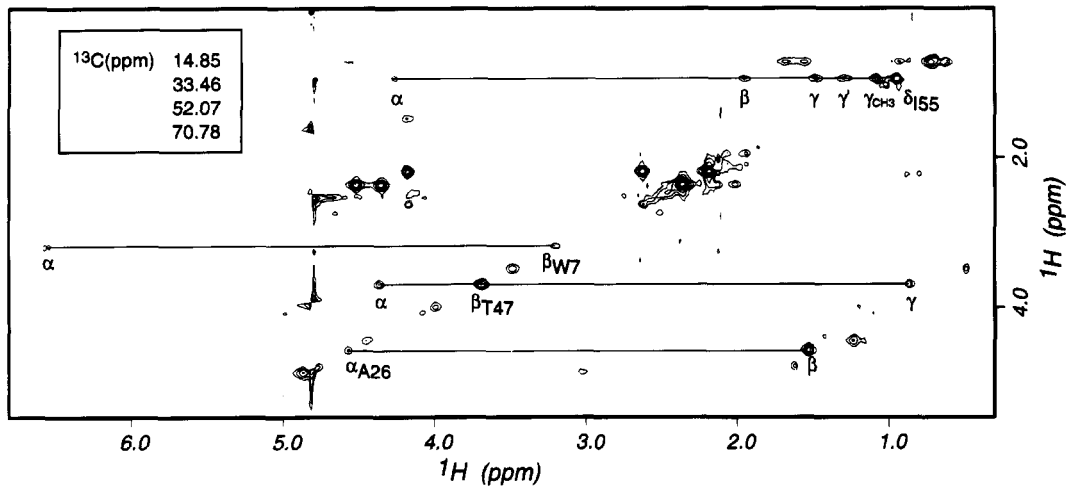

FIGURE 3: 2D ^{1}H−^{1}H plane of a 3D ^{13}C HCCH-TOCSY. Spin systems are labeled with residue assignment at the diagonal peak, with cross peaks labeled by proton type. Due to extensive aliasing in the F_2 dimension, the ^{13}Cδ of I55 at 14.85 ppm, the ^{13}Cβ of W7 at 33.46 ppm, and the ^{13}Cα of A26 at 52.07 ppm appear in the same plane as ^{13}Cβ of T47 at 70.78 ppm.

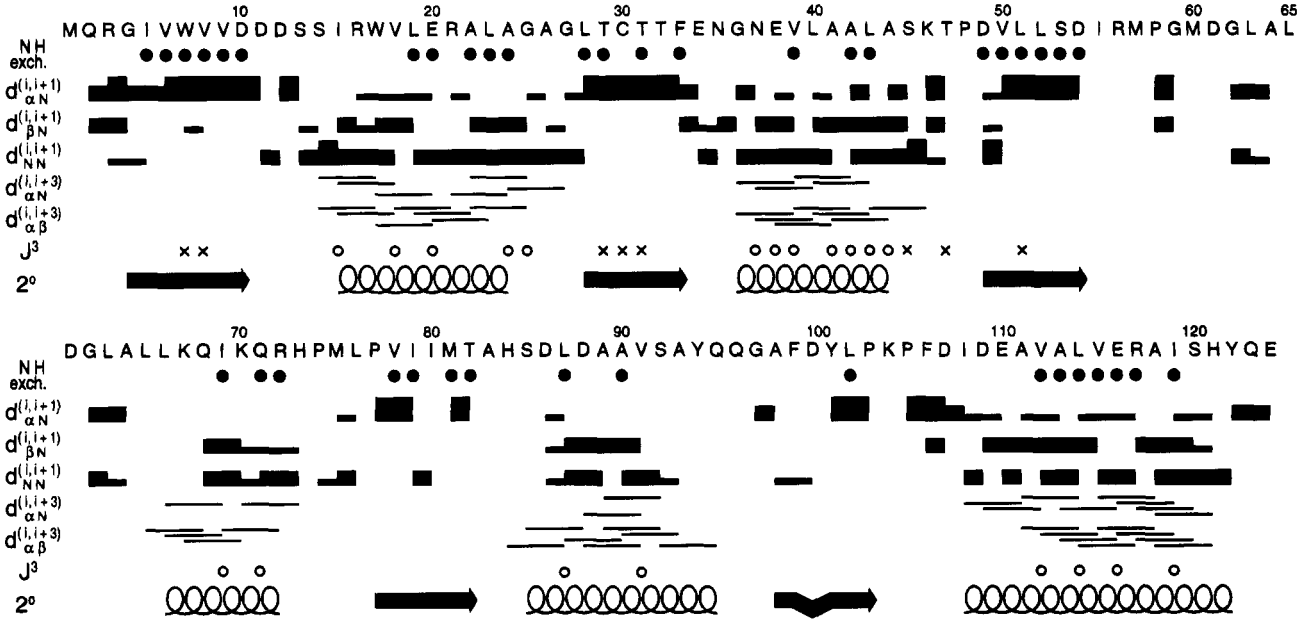

FIGURE 4: Summary of sequential and medium-range NOEs, slowly exchanging amide protons, and $J^3_{\alpha H-NH}$ values for NTRC receiver domain. The relative intensity of seqential NOEs is indicated by height of connecting box. Horizontal lines represent helical medium-range NOEs. Filled circles reflect amide protons which are observed in spectra collected at pH 6.4, 25 °C, at least 1 h after dissolving the sample in D_2O. Small (<6 Hz) and large (>9 Hz) values of $J^3_{\alpha H-NH}$ are represented by O and ×, respectively.

NOE information, as well as $J^3_{\alpha H-NH}$ coupling constant data and amide exchange information. Patterns of sequential βH−NH and NH−NH NOEs as well αH−NH(i,i+3) and αH−βH(i,i+3) NOEs indicate the presence of helices in the regions from residues 14−27, 36−44, 65−73, 85−95, and 108−121. Some αH−NH(i,i+3) NOEs for the start of helix 2 are highlighted in Figure 2. Strong sequential αH−NH NOEs indicate regions of extended conformation for the backbone of residues 2−11, 28−34, 50−54, 77−82, and 101−103. The large number of slowly exchanging amide protons in these regions suggests the presence of β-sheet structure.

Figure 5 shows the clear correlation of ^{13}Cα and ^{13}Cβ secondary shifts with the secondary structure elements of the NTRC receiver domain, especially when the differences between ^{13}Cα and ^{13}Cβ secondary shifts are examined in panel C. This agrees with the observed relationship between ^{13}Cα and ^{13}Cβ secondary shifts and location within an α-helix or β-sheet (Spera & Bax, 1991). The five regions of helical secondary shifts coincide with the pattern of helical NOEs shown in Figure 4, and the β-strands are in regions in which the trend of secondary shifts is reversed.

Helices are often bounded by initiation or termination signal sequences (Presta & Rose, 1988). The convention for specifying positions in and around helices is (...N″, N′, N-cap, N1, N2 ... C2, C1, C-cap, C′, C″...), with N-cap and C-cap denoting the first and last residues of the helix, respectively. Patterns of ^{13}Cα and ^{13}Cβ secondary shifts at the beginning of α-helices have been shown to indicate the presence of N-terminal helix capping interactions (Gronenborn & Clore, 1994). Close examination of the secondary shifts of the NTRC receiver domain indicates the possibility of capping interactions for helices 2 and 5, due to the characteristic downfield shift of the ^{13}Cβ resonances of the N-cap residues, N35 and D107, coupled with a slight shift upfield for the ^{13}Cα resonances of the same residues. The

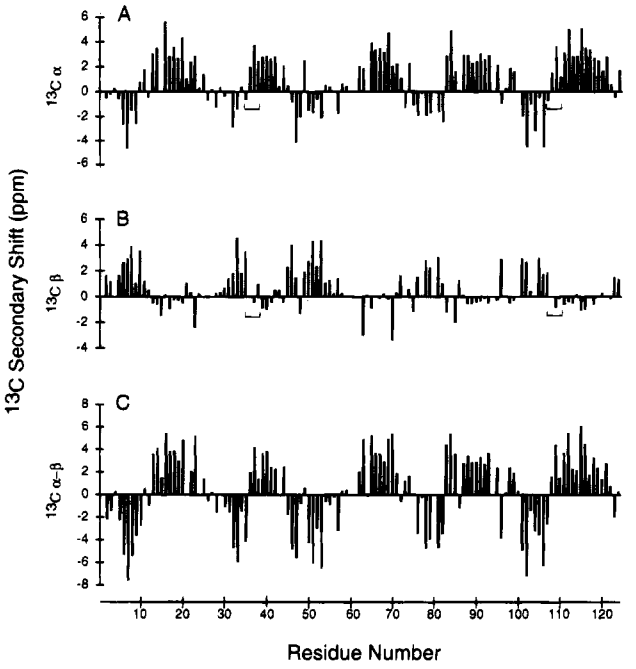

FIGURE 5: Observed ^{13}C secondary shifts of NTRC receiver domain, plotted as a function of residue number. Values reflect measured ^{13}C chemical shifts minus the amino acid-specific "random coil" ^{13}C chemical shift (Spera & Bax, 1991) in ppm, with positive and negative values indicating downfield and upfield secondary shifts, respectively. (A) $^{13}C\alpha$ secondary shifts. (B) $^{13}C\beta$ secondary shifts. (C) $^{13}C\alpha$ secondary shifts − $^{13}C\beta$ secondary shifts. Helical and extended regions are clearly evident in panel C as positive and negative regions, respectively. Patterns suggestive of helix N-capping interactions (Gronenborn & Clore, 1994) are marked with brackets in panels A and B (residues 35−38 and 107−110).

following three residues, at the N1−N3 positions of each helix, display downfield $^{13}C\alpha$ secondary shifts, in agreement with the reported pattern.

NOEs characteristic of N-terminal capping interactions have also been identified (Lyu et al., 1993; Zhou et al., 1994). NOEs are observed between Hβ resonances of the N3 residues, E38 and E110, and the backbone NH and side chain resonances of the capping residues, N35 and D107, respectively. Interestingly, the N3 residues for both helices, E38 and E110, are potential "capping box" residues, having the ability to accept a reciprocal hydrogen bond from the backbone NH of the N-cap residue (Harper & Rose, 1993). In contrast to helices 2 and 5, neither the $^{13}C\alpha$ and $^{13}C\beta$ secondary shifts nor the NOE data for the N-terminal residues of helix 1 provide evidence of N-capping, and helix capping interactions could not be identified for the N-terminal residues of helices 3 and 4, due to the lack of NOEs defining the initiation points of those helices.

One instance of C-terminal helix capping is observed for residues 23−28, as evidenced by the slow exchange of the backbone NH of L28 and a pattern of NOEs which results in the positioning of L28 NH within 3.5 Å of L23 CO, and G27 NH within 2.0 Å of A24 CO. Recently, the termination of α-helices involving glycine residues has been classified into two major motifs (Aurora et al., 1994). The sequence of residues for the C-cap of helix 1 follows the proposed rules for the Schellman motif, which require a glycine at the C′ position (G27) and apolar residues with hydrophobic contacts at the C3 and C″ positions (L23 and L28). This arrangement produces a 6−1 (L28−L23), 5−2 (G27−A24)

Table 1: Statistics for 20 NTRC Receiver Domain DGSA Structures[a]

restraint totals by type	number
long-range NOE	229
medium-range NOE	180
sequential NOE	213
intraresidue NOE[b]	194
hydrogen bond distance	82
dihedral	19
total restraints	917

X-PLOR energies (kcal/mol)	⟨SA⟩
E_{total}	322 ± 32
E_{bond}	13 ± 2
E_{angle}	189 ± 11
$E_{improper}$	25 ± 3
E_{vdw}[c]	42 ± 8
E_{noe}[d]	46 ± 11
E_{cdih}[e]	6.3 ± 1.7

RMSD from ideal geometry	⟨SA⟩
bonds (Å)	0.0026 ± 0.0002
angles (deg)	0.60 ± 0.02
impropers (deg)	0.41 ± 0.03

RMSD from experimental restraints	⟨SA⟩
distance restraints[f]	0.032 ± 0.004
dihedral restraints[f]	2.32 ± 0.30

atomic RMSDs (Å)	N, Cα, C, O	all non-H
⟨SA⟩ vs $\overline{\langle SA\rangle}_{2^\circ\ struct}$	0.81 ± 0.06	1.35 ± 0.11
⟨SA⟩ vs $\overline{\langle SA\rangle}_{all\ residues}$	1.50 ± 0.12	2.13 ± 0.09

[a] Notation is as follows: ⟨SA⟩ is the ensemble of 20 final XPLOR structures. $\overline{\langle SA\rangle}_{2^\circ\ struct}$ is the average coordinates for residues involved in secondary structure (4−10, 14−44, 48−55, 65−73, and 98−122) which were obtained from a least-squares superposition of of those backbone (N, Cα, C, O) heavy atoms. $\overline{\langle SA\rangle}_{all\ residues}$ is the average coordinates for residues 1−124 obtained from a least-squares superposition of those backbone heavy atoms. [b] Intraresidue restraints were included for NOEs between side chain protons which were more than four bonds apart. [c] The X-PLOR F_{repel} function was used to simulate the van der Waals potential with atomic radii ranging from 0.9 times their CHARMM (Brooks et al., 1983) values at high temperatures to 0.75 their CHARMM values at low temperatures (Brünger, 1992). [d] NOE-derived distance restaints were applied with a square-well potential with force constants of 50 kcal mol^{-1} Å^{-2}. [e] Dihedral angles were given force constants of 200 kcal mol^{-1} rad^{-2} which were applied at the beginning of the annealing/refinement stage. [f] A majority of NOE violations involved medium-range restraints in helix 4. A total of two NOE violations greater than 0.5 Å were found in the family of 20 accepted structures, and one dihedral restraint violation of greater than 6° was observed.

hydrogen bonding arrangement resulting in energetically favorable helix termination (Schellman, 1980).

Figure 6 displays the arrangement of the parallel β-sheet of NTRC receiver domain, as indicated by long-range NOEs, and the pattern of solvent-protected backbone amide protons. The five-stranded sheet has regular patterns of cross-strand connectivities, including αH−NH, αH−αH, and NH−NH NOEs. Examples of cross-strand αH−NH NOEs can be seen in Figure 2. The N-terminal residue of strand 3, D49, plays an unusual role in the β-sheet. The NH of D49, while protected from solvent exchange, has NOEs to I5 NH and V50 NH. The I5 NH, which is also protected, has NOEs to the βH resonances of D49. In structure calculations without hydrogen bond restraints for these residues, the CO of I5 is reproducibly positioned so as to form hydrogen bonds with

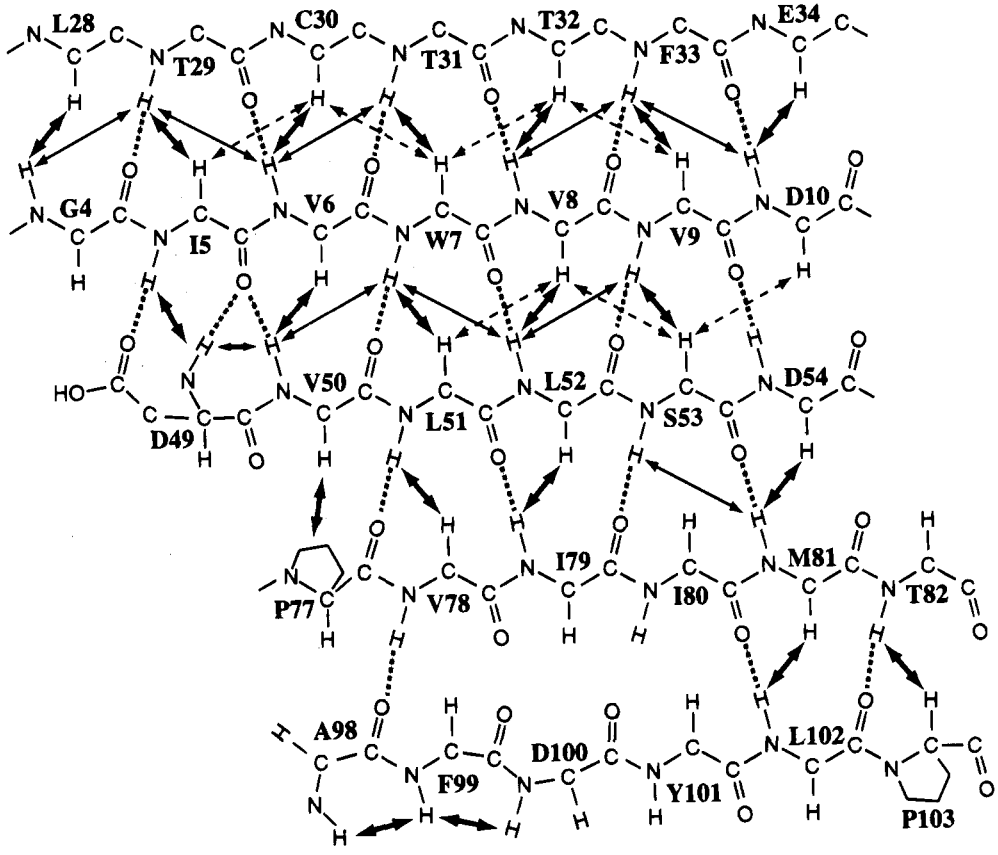

FIGURE 6: Cross-strand NOEs and hydrogen bonds observed for the β-sheet of NTRC receiver domain. Solid arrows correspond to NOEs observed in 3D ^{15}N NOESY-HMQC and dashed arrows correspond to NOEs observed in 2D ^{1}H$-^{1}$H NOESY. Dashed lines indicate hydrogen bonds included in structure calculations involving amide protons with reduced exchange rates.

both D49 NH and V50 NH in a backbone conformation commonly characterized as a β-bulge (Richardson, 1981). At the same time, the side chain CO of D49 is found to be the obvious acceptor for a hydrogen bond from I5 NH, appearing at an average distance of less than 3.0 Å. On the basis of these preliminary calculations, hydrogen bond restraints for these residues were included in the late rounds of refinement.

A β-bulge is also evident in strand 5. NOE patterns and amide exchange data indicate normal β-sheet hydrogen bonding between residues 81−102 and 82−103, but a lack of NOEs and amide protection for the preceding residues of strand 5 prevents the assignment of hydrogen bonds between 80−101 and 79−100. Additionally, the pattern of sequential NOEs for residues 98−100 is not consistent with extended β-sheet structure. NH−NH NOEs from 98 to 99 and 99 to 100 and a lack of strong sequential αH−NH NOEs reduce the likelihood of normal β-sheet formation for those residues. The NH of V78 is also protected from exchange, and the CO of A98 was determined to be its hydrogen bond acceptor. NOEs from the side chains of F99 and Y101 position the residues of the bulge adjacent to strand 4, but without the backbone interactions typical of β-sheet structures.

Determination of the Three-Dimensional Structure of NTRC Receiver Domain. Table 1 summarizes the statistics of structure calculations of the NTRC receiver domain. Distance restraints for the structure calculations of NTRC receiver domains were generated from ^{15}N-edited and ^{13}C-edited spectra, as described in Materials and Methods. A total of 915 experimental restraints were used, including 816 NOE-derived distance restraints, 19 dihedral angle restraints from the HMQC-J spectrum, and 80 restraints defining 40 hydrogen bonds. A total of 30 structures were calculated using the program X-PLOR 3.1. Of the 30 calculated structures, 20 with low final energies and minimal distance restraint violations were chosen for evaluation. Superposition of the residues contained in secondary structure, excluding helix 4, yields average root mean square deviations from the average of 0.81 Å for the backbone atoms and 1.35 Å for non-hydrogen atoms. Figure 7 shows the family of 20 structures superimposed on the backbone atoms of the average structure. The ensemble reflects a single well-defined fold, with the loop from R56 to A64 being the most poorly defined region.

The $(\beta/\alpha)_5$ fold of the NTRC receiver domain has topological similarity to other α/β protein structures (Richardson, 1981), with helices 1 and 5 nearly orthogonal to each other on one face of the sheet and helices 2, 3, and 4 lying roughly parallel to each other on the other face. A number of hydrophobic interactions between the β-sheet and the helices are indicated by NOEs between side chains of aliphatic and aromatic residues. One pocket of hydrophobic interactions involves residues V115 and I119 in helix 5, which have multiple NOE contacts to I79, L52, and V50. These interactions are important for defining the position of helix 5 next to the β-sheet. Another group of side chains including C30, L28, L23, and E20 is sufficiently buried to protect the sulfhydryl proton of C30 from rapid solvent exchange, allowing the normally unobserved resonance to be detected, even in experiments with presaturation of the solvent H_2O signal.

FIGURE 7: Family of 20 distance geometry-simulated annealing structures of NTRC receiver domain. Structures are superimposed on backbone atoms of the average structure, including residues 4−10, 14−44, 48−55, 65−73, 77−82, and 98−121.

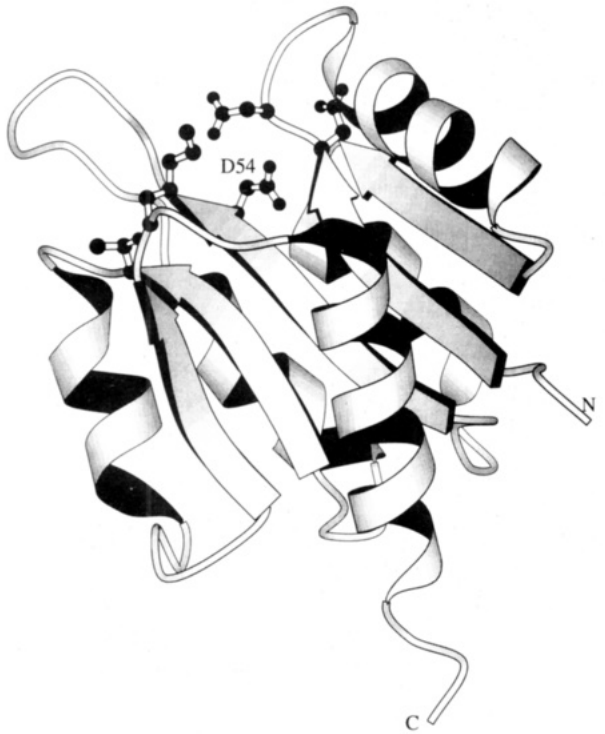

FIGURE 8: Ribbon diagram of the NTRC receiver domain, drawn on the structure with lowest RMSD to the average structure with the program Molscript (Kraulis, 1991). Helices are represented by flat ribbons and β-strands are indicated by arrows pointing N-terminus to C- terminus. Active-site residue side chains are shown: D10, D11, D54, T82, K104.

A ribbon diagram of the NTRC receiver domain is shown in Figure 8. Conserved residues of the active site form a cluster of side chains at the C-terminal ends of the β-strands. The side chain of D54 is the site of phosphorylation. The side chains of residues D10, D54, and T82 are in close proximity due to their locations in the sheet. The ζNH_3^+ of K104 is oriented toward the side chain of D54, but the complete degeneracy of the D54 $^1H\beta$ and $^{13}C\beta$ resonances with the K104 $^1H\epsilon$ and $^{13}C\epsilon$ resonances prevents the unambiguous assignment of NOEs which might position the K104 side chain more precisely in the active site. The position of the side chain of D11 is not well-defined in the family of structures due also to a lack of NOEs for that residue.

DISCUSSION

The N-terminal receiver domain of the NTRC protein has been expressed at high levels and uniformly ^{15}N- and ^{13}C-labeled. The ^1H, ^{15}N, and ^{13}C resonance assignments have been completed using 3D ^{15}N- and ^{13}C-edited NMR techniques. Distance information was derived from 3D ^{15}N-edited NOESY-HMQC and 4D ^{13}C-edited HMQC-NOESY-HMQC spectra, while coupling constant and amide exchange information came from 2D $^{15}N-^1H$ experiments. The three-dimensional structure of the NTRC receiver domain was calculated using hybrid distance geometry/simulated annealing (DGSA) techniques. This structure provides a starting point from which to examine the effects of Mg^{2+} and phosphorylation on the NTRC receiver domain, and its subsequent interaction with the central domain of NTRC.

Comparison of NTRC Receiver Domain with CheY. High-resolution structures of CheY, a homologous receiver domain protein, have been determined by X-ray crystallography in the absence (Volz & Matsumura, 1991) and presence of Mg^{2+} (Stock et al., 1993; Bellsolell et al., 1994). Overall similarity between the NTRC receiver domain and CheY is high, as would be expected from the high degree of sequence conservation [29% identity for the proteins from enteric bacteria (Volz, 1993)]. Superposition of only the residues of the β-sheet of the average NTRC receiver domain structure on each of the three high-resolution structures of CheY yields RMS deviations in Cα positions of 1.3 Å. All further comparisons of NTRC receiver domain to CheY were found to be identical for the three CheY structures.

There are two insertions in CheY relative to NTRC, but neither seems to have important structural consequences. Helix 3 of CheY has one extra turn at the C-terminus compared to helix 3 in the NTRC receiver domain, due to the presence of two additional residues in CheY in this region and the termination of this helix in NTRC by P74. The other residue insertion in CheY relative to NTRC occurs between helix 1 and strand 2, just after the C-cap of helix 1, but has no significant effect upon the positioning of structural elements. Orientations of helices 1, 2, 3, and 5 relative to the sheet are generally similar in the NTRC receiver domain and CheY. The Cα RMSD between the average NTRC structure and CheY is 2.7 Å for superposition of the sheet and helices 1, 2, 3, and 5.

Strikingly, inclusion of helix 4 in the superposition raises the RMSD value to 3.5 Å. When CheY and the NTRC

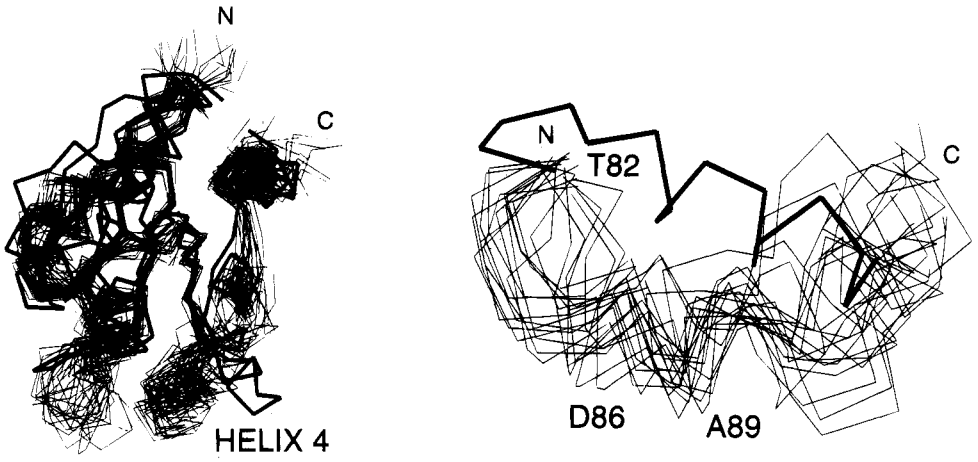

FIGURE 9: Superposition of 20 NTRC receiver domain structures on the high-resolution crystal structure of CheY. The following residues were used for the alignment of structures: NTRC, 4−10, 15−45, 49−55, 66−72, 76−82, 97−122; CheY, 6−12, 17−30, 32−48, 52−58, 69−75, 81−87, 102−127. Cα traces of the full structures (A) and helix 4 in detail (B) are shown. The approximate locations of key residues from NTRC are indicated.

receiver domain are superimposed on all secondary structural elements except helix 4, a difference in the orientation of the helix 4 axes of approximately 45° is observed. Figure 9a shows the superposition of the 20 DGSA structures of the NTRC receiver domain on the Cα trace of the crystal structure of CheY in the absence of Mg^{2+} (Brookhaven PDB file 3CHY). Average displacements from the corresponding CheY Cα coordinates of 8.1−9.5 Å are observed for the Cα atoms of residues L87−A90 of NTRC. The RMS deviations of those four Cα atoms from the average NTRC receiver domain structure range from 1.3 to 1.8 Å, significantly smaller than the observed differences from CheY. While helical NOEs are observed for residues 85−95 in the NTRC receiver domain (see Figure 4), fewer long-range restraints were identified between these residues and the rest of the protein, resulting in higher local RMS deviations. Figure 9b illustrates in detail the difference in position of helix 4 in CheY and the family of NTRC structures. The range of coordinates spanned by residues 85−90 in the ensemble of NTRC structures clearly does not overlap the position of the same residues in CheY.

Active-Site Residues. The five conserved active site residues of the receiver domain superfamily are present in NTRC as well: D10, D11, D54, T82, and K104 (Moore et al., 1993). The resolution of this structure does not permit close comparison of these side chains with the corresponding groups in CheY. However, the proximal positions of these residues in the structure of the NTRC receiver domain are consistent with their involvement in Mg^{2+} binding and phosphorylation.

Helix Capping. The Schellman C-terminal capping motif identified in helix 1 in the NTRC receiver domain is also present in the CheY structures. Examination of the sequence alignment for the receiver domain superfamily (Volz, 1993) reveals the conservation of the C′ glycine and the apolar residues at the C3 and C″ positions, in accordance with the stereochemical rules for Schellman motifs (Aurora et al., 1994). The C3 position is a leucine in the consensus sequence, and the C″ position is always an apolar residue, if the conserved glycine is present. The solvent-exposed C1 position is a polar residue in nearly 90% of the sequences. Mutation of key Schellman motif residues (C3, C′, or C″) can be very destabilizing, as seen in Staphylococcal nuclease (Shortle et al., 1990; Green et al., 1992). The conservation in the superfamily at these positions can be explained by the energetically favorable termination of helix 1 afforded by this C-capping motif.

The N-caps for helices 2 and 5 which are suggested by the data for NTRC receiver domain are present in the crystal structures of CheY. The distances from the side chain oxygen atoms of D38 and T112 to the amide nitrogens of D41 and T115 are 2.9 and 3.2 Å, respectively. No single residue type appears to be conserved at these capping positions in the CheY superfamily sequences. However, when all possible N-capping residues (S, T, D, N, E, Q, H, and C) are considered, a trend emerges. A potential N-cap for helix 2 is found in 86% of sequences, and in 65% of the sequences for helix 5. It is also interesting to consider the possibility of conserved "capping box" motifs (Harper & Rose, 1993). Conservation of capping box partners (N-cap and N3 position) is lower, but still significant: 59% for helix 2, and 46% for helix 5. Like the C-capping motifs, N-capping interactions provide an energetically favorable helix termination, forming one (N-cap) or two (capping box) additional hydrogen bonds which would otherwise be unsatisfied and are a structural motivation for conservation at the N-cap and N3 positions.

β-Bulges. The β-bulge and hydrogen bonding pattern at D49 in strand 3 of the NTRC receiver domain clarifies the basis for conservation at that position throughout the superfamily. The side chain of D49 forms a cross-strand hydrogen bond to a backbone NH of strand 1, providing an additional stabilizing force at the N-terminal end of the β-sheet. This type of interaction may be present in other (α/β) proteins where aspartic acid is the most common N-terminal residue in β-strands (Colloc'h & Cohen, 1991). A similar side chain interaction is found in strand 5 in CheY, where a serine hydroxyl at the start of strand 5 accepts a hydrogen bond from a backbone amide in strand 4. The subsequent bulge is present in both NTRC and CheY, but the N-terminal residue of strand 5 in the NTRC receiver domain, A98, forms a normal backbone hydrogen bond to strand 4.

Function of Helix 4 in the Receiver Domain of NTRC. As discussed above, helix 4 is the only structural element of the receiver domain of NTRC that is significantly repositioned with respect to CheY. Interestingly, two of the three

"constitutive" amino acid substitutions so far identified in the receiver domain of NTRC (D86N and A89T) affect residues in helix 4 (Y. Flashner, J. Keener, and S. Kustu, unpublished results). The third substitution, D54E, affects the site of phosphorylation (Klose et al., 1993). NTRC constitutive proteins have some ability to activate transcription without being phosphorylated, both in vivo and in vitro. Hence, constitutive substitutions, which mimic phosphorylation, provide evidence for the functional importance of helix 4. It will be of interest to determine the relationship between structural changes in constitutive forms of the NTRC receiver domain and those that occur upon phosphorylation of the wild-type domain. The only constitutive substitutions known in CheY, D13K/R, appear to cause only local structural perturbations, whereas changes which occur upon phosphorylation of wild-type CheY are global (Bourret et al., 1993).

ACKNOWLEDGMENT

We thank Andrew Lee for invaluable assistance with four-dimensional data analysis, Biosym for providing β-test versions of FELIX, Anne North for performing enzymatic activity assays, David King for performing electrospray mass spectrometry, and Mark Coy and Ken Stedman for critical reading of the manuscript.

SUPPLEMENTARY MATERIAL AVAILABLE

One table containing the ^{1}H, ^{15}N, and ^{13}C chemical shift assignments for the NTRC receiver domain, pH 6.4, at 25 °C (6 pages). Ordering information is given on any current masthead page.

REFERENCES

Aurora, R., Srinivasan, R., & Rose, G. D. (1994) *Science 264*, 1126−1130.

Austin, S., & Dixon, R. (1992) *EMBO J. 11*, 2219−2228.

Bax, A., Clore, G. M., & Gronenborn, A. M. (1990) *J. Magn. Reson. 88*, 425−431.

Bellsolell, L., Prieto, J., Serrano, L., & Coll, M. (1994) *J. Mol. Biol. 238*, 489−495.

Bodenhausen, G., & Ruben, D. J. (1980) *Chem. Phys. Lett. 69*, 185−189.

Bourret, R. B., Drake, S. K., Chervitz, S. A., Simon, M. I., & Falke, J. J. (1993) *J. Biol. Chem. 268*, 13089−96.

Brooks, B. R., Bruccoleri, R. E., Olafson, B. D., States, D. J., Swaminathan, S. & Karplus, M. (1983) *J. Comput. Chem. 4*, 187−217.

Brünger, A. T. (1992) *X-PLOR Manual Version 3.1*, Yale University Press, New Haven, CT.

Chang, C., Kwok, S. F., Bleecker, A. B., & Meyerowitz, E. M. (1993) *Science 262*, 539−544.

Clore, G. M., Nilges, M., Sukumaran, D. K., Brünger, A. T., Karplus, M., & Gronenborn, A. M. (1986) *EMBO J. 5*, 2729−2735.

Clore, G. M., Kay, L. E., Bax, A., & Gronenborn, A. M. (1991) *Biochemistry 30*, 12−18.

Colloc'h, N., & Cohen, F. E. (1991) *J. Mol. Biol. 221*, 603−613.

Dorman, D. E., & Bovey, F. A. (1973) *J. Org. Chem. 38*, 2379−2383.

Driscoll, P. C., Clore, G. M., Marion, D., Wingfield, P. T., & Gronenborn, A. M. (1990) *Biochemistry 29*, 3542−3556.

Drummond, M. H., Conteras, A., & Mitchenall, L. A. (1990) *Mol. Microbiol. 4*, 29−37.

Feng, J., Atkinson, M., McCleary, W., Stock, J., Wanner, B., & Ninfa, A. (1992) *J. Bacteriol. 174*, 6061−6070.

Green, S. M., Meeker, A. K., & Shortle, D. (1992) *Biochemistry 31*, 5717−5728.

Gronenborn, A. M., & Clore, G. M. (1994) *J. Biomol. NMR 4*, 455−458.

Grzesiek, S., & Bax, A. (1992) *J. Am. Chem. Soc. 114*, 6291−6293.

Harper, E. T., & Rose, G. D. (1993) *Biochemistry 32*, 7605−7609.

Hess, J. F., Oosawa, K., Kaplan, N., & Simon, M. I. (1988) *Cell 53*, 79−87.

Kay, L. E., & Bax, A. (1990) *J. Magn. Reson. 86*, 110−126.

Kay, L. E., Marion, D., & Bax, A. (1989) *J. Magn. Reson. 84*, 72−84.

Keener, J., & Kustu, S. (1988) *Proc. Natl. Acad. Sci. U.S.A. 85*, 4976−4980.

Klose, K. E., Weiss, D. W., & Kustu, S. (1993) *J. Mol. Biol. 232*, 67−78.

Klose, K., North, A., Stedman, K., & Kustu, S. (1994) *J. Mol. Biol. 240* (in press).

Kraulis, P. J. (1991) *J. Appl. Crystallogr. 24*, 946−950.

Live, D. H., Davis, D. G., Agosta, W. C., & Cowburn, D. (1984) *J. Am. Chem. Soc. 106*, 1934−1941.

Lukat, G. S., Lee, B. H., Mottonen, J. M., Stock, A. M., & Stock, J. B. (1991) *J. Biol. Chem. 266*, 8348−8354.

Lukat, G. S., McCleary, W. R., Stock, A. M., & Stock, J. B. (1992) *Proc. Natl. Acad. Sci. U.S.A. 89*, 718−722.

Lyu, P. C., Wemmer, D. E., Zhou, H. X., Pinker, R. J., & Kallenbach, N. R. (1993) *Biochemistry 32*, 421−425.

Maeda, T., Wurgler-Murphy, S. M., & Saito, H. (1994) *Nature 369*, 242−245.

Manoleras, N., & Norton, R. S. (1992) *J. Biomol. NMR 2*, 485−494.

Marion, D., Ikura, M., Tschudin, R., & Bax, A. (1989a) *J. Magn. Reson. 85*, 393−399.

Marion, D., Kay, L. E., Sparks, S. W., Torchia, D. A., & Bax, A. (1989b) *J. Am. Chem. Soc. 111*, 1515−1517.

Moore, J. B., Shiau, S. P., & Reitzer, L. J. (1993) *J. Bacteriol. 175*, 2692−2701.

Moy, F. J., Lowry, D. F., Matsumura, P., Dahlquist, F. W., Krywko, J. E., & Domaille, P. J. (1994) *Biochemistry 33*, 10731−10742.

Nilges, M., Clore, G. M., & Gronenborn, A. M. (1988) *FEBS Lett. 229*, 317−324.

Ninfa, A. J., & Magasanik, B. (1986) *Proc. Natl. Acad. Sci. U.S.A. 83*, 5909−5913.

Ota, I. M., & Varshavsky, A. (1993) *Science 262*, 566−569.

Parkinson, J. S., & Kofoid, E. C. (1992) *Annu. Rev. Genet. 26*, 71−112.

Porter, S. C. (1993) Ph.D. Thesis, University of California, Berkeley, Berkeley, CA.

Porter, S. C., North, A. K., & Kustu, S. (1995) in *Two-Component Signal Transduction* (Silhavy, T., & Hoch, J., Eds.) American Society of Microbiology, Washington, D.C.

Presta, L. G., & Rose, G. D. (1988) *Science 240*, 1632−1641.

Ravid, S., Matsumura, P., & Eisenbach, M. (1986) *Proc. Natl. Acad. Sci. U.S.A. 83*, 7157−7161.

Richardson, J. S. (1981) *Adv. Protein Chem. 34*, 167−337.

Sambrook, J., Fritsch, E. F., & Maniatis, T. (1989) *Molecular Cloning: A Laboratory Manual*, Cold Spring Harbor Laboratory Press, Cold Spring Harbor, NY.

Sanders, D. A., Gillece-Castro, B. L., Burlingame, A. L., & Koshland, D. E., Jr. (1992) *J. Bacteriol. 174*, 5112−5122.

Scanlon, M. J., & Norton, R. S. (1994) *Protein Sci. 3*, 1121−1124.

Schellman, C. (1980) in *Protein Folding* (Jaenicke, R., Ed.) pp 53−61, Elsevier, North-Holland, New York.

Shortle, D., Stites, W. E., & Meeker, A. K. (1990) *Biochemistry 29*, 8033−8041.

Spera, S., & Bax, A. (1991) *J. Am. Chem. Soc. 113*, 5490−5492.

Stock, A. M., Mottonen, J. M., Stock, J. B., & Schutt, C. E. (1989) *Nature 337*, 745−749.

Stock, A. M., Martinez-Hackert, E., Rasmussen, B. F., West, A. H., Stock, J. B., Ringe, D., & Petsko, G. A. (1993) *Biochemistry 32*, 13375−13380.

Studier, F. W., Rosenberg, A. H., Dunn, J. J., & Dubendorff, J. W. (1990) *Methods Enzymol. 185*, 60−89.

Volz, K. (1993) *Biochemistry 32*, 11741−11753.

Volz, K., & Matsumura, P. (1991) *J. Biol. Chem. 296*, 15511−15519.

Vuister, G. W., & Bax, A. (1992) *J. Magn. Reson. 98*, 428−435.

Weiss, D. S., Batut, J., Klose, K. E., Keener, J., & Kustu, S. (1991) *Cell 67*, 155−167.

Weiss, D. S., Klose, K. E., Hoover, T. R., North, A. K., Porter, S. C., Wedel, A. B., & Kustu, S. (1992) in *Transcriptional Regulation* (McKnight, S. L., & Yamamoto, K. R., Eds.) pp 667−694, Cold Spring Harbor Laboratory Press, Cold Spring Harbor, NY.

Weiss, V., & Magasanik, B. (1988) *Proc. Natl. Acad. Sci. U.S.A. 85*, 8919−8923.

Weiss, V., Claverie-Martin, F., & Magasanik, B. (1992) *Proc. Natl. Acad. Sci. U.S.A. 89*, 5088−5092.

Williamson, M. P., Havel, T. F., & Wüthrich, K. (1985) *J. Mol. Biol. 182*, 295−315.

Wüthrich, K. (1976) *NMR in Biological Research: Peptides and Proteins*, North Holland, Amsterdam.

Wüthrich, K. (1986) *NMR of Proteins and Nucleic Acids*, John Wiley & Sons, New York.

Wüthrich, K., Billeter, M., & Braun, W. (1983) *J. Mol. Biol. 169*, 949−961.

Zhou, H. X., Lyu, P. C., Wemmer, D. E., & Kallenbach, N. R. (1994) *Proteins: Struct., Funct., Genet. 18*, 1−7.

BI942196J